applied sciences

MDPI

Article

Effects of the Projectile Geometries on Normal and Oblique Penetration Using the Finite Cavity Pressure Method

Yo-Han YOO [1], Jong-Bong KIM [2] and Chang-Whan LEE [3,*]

[1] The 4th Research and Development Institute, Agency for Defense Development, Daejeon 34186, Korea; yyhh1986@add.re.kr

[2] Department Mechanical and Automotive Engineering, Seoul National University of Science and Technology (SeoulTech), Seoul 01811, South Korea; jbkim@seoultech.ac.kr

[3] Department of Mechanical System Design Engineering, Seoul National University of Science and Technology (SeoulTech), Seoul 01811, South Korea

* Correspondence: cwlee@seoultech.ac.kr; Tel.: +82-2-970-6371

Received: 14 August 2019; Accepted: 16 September 2019; Published: 19 September 2019

Abstract: In this work, the penetration depth of a projectile with various geometries was analyzed using the cavity pressure method. The finite cavity method combines an analytical method and the finite element method and considers the deformation of the projectile only. This simulation method was implemented to ABAQUS/Explicit using user subroutine VDLOAD. The target material was 6061-T6511 aluminum material, and the projectile material was vacuum-arc-remelted (VAR) 4340 steel. In the analysis, the normal impact and the oblique impact with the angle of 30° were studied. First, the developed simulation model was verified using the previous experiments. With the developed finite element analysis with the cavity pressure method, the effect of projectile shape on penetration was investigated. The target geometry maximizes penetration depth was discussed. The angle of the nose affects mainly on the penetration characteristics. The projectile having an ogive nose with high caliber-radius-head (CRH) value shows the best penetration depth and the least plastic deformation in both the normal impact and the oblique impact.

Keywords: projectile; nose geometry; cavity pressure

1. Introduction

Predicting the penetration depth of the projectile is one of the essential aspects of the geometric design of the projectile [1]. In particular, projectiles are expensive, preparation and experiments of projectiles take so much time and cost. Additionally, the effects of design variables are challenging to study accurately due to measuring errors and experiment problems.

Recent developments in computational capabilities and techniques have made computational simulation very efficient in many ways [2,3]. Simulation considering deformation of the projectile and the target costs too much computational time. Also, the deformation and fracture characteristics of the target and the contact problem between the target and the projectile are required [4].

Thus, a theoretical and empirical based model for penetration has been developed for rapid prediction. Young [5] developed an empirical-based simple analytic equation for predicting the penetration depth of the projectile. Young's equation was derived based on the energy method and some empirical variables. The advantage of Young's equation is that the calculation time is short, and the use is simple. However, in the calculation, the deformation of the projectile is not calculated. It is difficult to apply to various environments.

Another method considering lateral loading was developed based on Young's equation [6]. The calculation was completed with small time increments. The reaction forces were calculated from Young's equation and applied to the projectile with an explicit method. However, it was not possible to consider the change of the reaction force with respect to deformation of the projectile.

The cavity pressure method [7–9] is an analytical method that calculates the reaction forces resulting from targets with respect to the expansion speed of the cavity. Normal pressure on the projectile nose is approximated by the results from the radial stress on the cavity surface. Forrestal and Luk [7] developed penetration equations for soil targets with Mohr-Columb and Tresca yield criteria. According to the yield criteria, the boundary condition of the elastic-plastic interface is different. Forrestal and Tzou [8] developed a spherical cavity-expansion penetration model for concrete targets for an incompressible and compressible material. Warren and Forrestal [10] derived a spherical cavity pressure distribution of the aluminum plate, considering compressible, strain hardening, and strain-rate dependence. The integration of the projectile surface with the cavity pressure presents axial reaction forces. From Newton's law, the acceleration and the penetration depth of the projectile were calculated. However, the cavity pressure method cannot consider the deformation of the projectile. When the deformation of the projectile is extensive (i.e., aluminum target), the cavity pressure method is not proper.

There have been some studies regarding the effects of the projectile geometries. Chen and Li [11] studied the effect of a non-deformable projectile having different geometrical characteristics on the penetration with the cavity expansion method. A general geometry function was introduced to define the geometrical characteristics of the projectile. When deformation of the projectile is very small, the prediction of the penetration using the cavity-expansion method is appropriate. He et al. [12] studied the penetration and perforation of the fiber-reinforced plastic (FRP) laminate with rigid projectiles.

The finite cavity method [13] is a method that links the advantages of finite element analysis with the advantages of analytical methods. Cavity pressure calculates the pressure distribution at this point when the point moves at a certain speed and calculates the reaction forces of the projectile. Finite element analysis was applied to predict the deformation and trajectory of the projectile. Fang et al. [14] and Kong et al. [15] conducted simulations of the projectile to consider the free-surface effect and the multi-layer effect with the finite cavity pressure method. It was found that the simulation was efficient and showed good agreements with the experimental results.

In this study, the penetration depth of a projectile was predicted using the finite cavity pressure method. In particular, the penetration depth with respect to the projectile geometry was analyzed using the finite cavity pressure method. Projectiles with a cylindrical geometry, a conical geometry, and an ogive nose were compared in the normal and oblique impacts. Through this study, the relationship between the deformation and the penetration depth of the projectile was analyzed. The relationship of the projectile geometry that can increase the penetration depth was studied.

2. Prediction of Penetration Depth Using the Finite Cavity Pressure Method

2.1. Cavity Pressure Method

Analytic calculation methods for penetration depth began with Bishop et al. [16]. Spherical cavity expansion models approximate a two-dimensional target response with equations derived from cavity expansion analyses. A schematic figure of the cavity pressure at the tip is shown in Figure 1. A spherical cavity expanded from the initial radius with a constant velocity V. As the spherical cavity expands, response regions were developed following plastic and elastic response regions [9,10]. The distribution of the cavity pressure is shown in Figure 2. The plastic region starts at the radius of b, and the elastic region begins at the radius of d. Cavity pressure was employed as an equation of penetration equations. From the equations of momentum and mass conservation with spherical symmetry, the pressure distribution can be calculated.

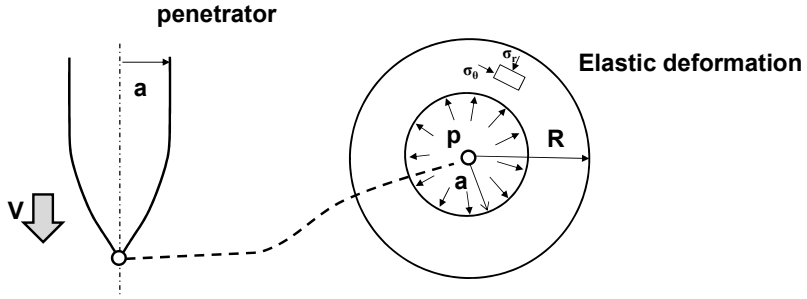

Figure 1. Expansion of the cavity pressure at the projectile tip.

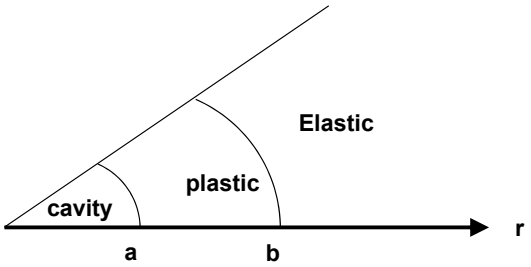

Figure 2. Distribution of the cavity pressure at the projectile tip.

The cavity pressure model depends on the target material property. Therefore, an appropriate cavity pressure model should be used. In this work, the target material was a 6061-T6511 aluminum plate. For this material, the compressible cavity pressure model considering strain hardening and strain rate dependency can precisely predict the response of the material [10]. Instead of using complex equations, the cavity pressure model was approximated with a second-order equation [10]. From the least square fit to the calculated pressure distribution with respect to the particle velocity (v), a normalized equation in Equation (1) was obtained.

$$\frac{\sigma_r}{Y} = A + B\left(\sqrt{\frac{\rho_0}{Y}}v\right) + C\left(\sqrt{\frac{\rho_0}{Y}}v\right)^2 \quad (1)$$

In Equation (1), v is the expansion speed of the cavity; Y is the yield stress of the target material; ρ_0 is the density of the material; A, B, and C are fitting coefficients. According to the material property and material model, the values of coefficients are varying. The value of coefficients of A, B, and C for a 6061-T6511 aluminum considering strain hardening and strain rate dependency are 5.039, 0.983, and 0.940, respectively. This model is suitable for 300 m/s to 1200 m/s [10]

2.2. Finite Cavity Pressure Method

The finite cavity pressure method is an application method for predicting the penetration depth of a projectile. The main difference between the analytical method using cavity pressure and the finite cavity pressure method is that the deformable projectile is employed and the pressure is applied to each element of the projectile in the finite cavity pressure method. The pressure normal to the surface of the projectile acts as a reaction pressure to penetration into the target. The projectile was modeled as a solid element such as hexahedral elements. As a result, the deformation and kinetics of the projectile can be calculated. The pressure was assumed to be applied to each node of the element, as shown in Figure 3 and applied in the finite element analysis as a boundary condition.

$$\frac{\sigma_r}{Y} = A + B\left(\sqrt{\frac{\rho_0}{Y}}\right)(\vec{V}\cdot\vec{n}) + C\left(\sqrt{\frac{\rho_0}{Y}}\right)^2(\vec{V}\cdot\vec{n})^2 \quad (2)$$

Equation (2) presents the pressure at each node where $\vec{V}$ is the nodal velocity, $\vec{n}$ is the unit normal vector of the corresponding element. Y_0 is the yield stress of the material, and ρ_0 is the density of the projectile material. Coefficients such as *A*, *B*, and *C* are defined from the cavity pressure method. In this work, the target was the aluminum plate. The cavity pressure of the previous work [17] was employed.

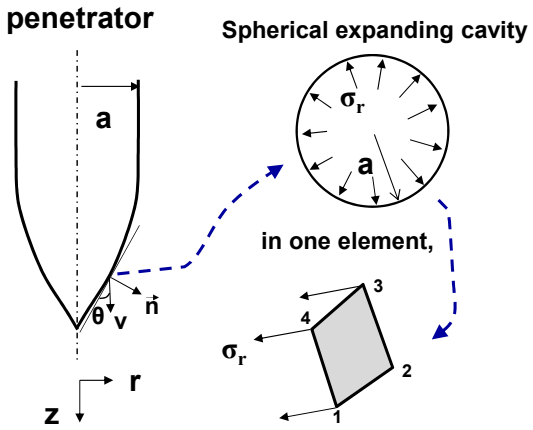

Figure 3. Schematic figure of the finite cavity pressure method.

The effective velocity of the element was defined as $\vec{V} \cdot \vec{n}$, which means the dot product of the element normal direction and the velocity vector of the node. For example, if the angle between the normal direction of the element and the velocity of the projectile is perpendicular, the effective velocity is zero. Consequently, no pressure is applied to the element. In this work, the finite cavity pressure method was employed in the ABAQUS/Explicit using the user load subroutine VDLOAD. User subroutine VDLOAD defines the magnitude of the distributed load as a function of position, velocity, and time. The calculating procedures are as follows: First, the velocity and the normal direction of the projectile were calculated. Next, the corresponding cavity pressure (σ_r) was calculated. Finally, the deformation of the projectile was calculated.

In the full simulation model, the projectile and the target should be modeled with very fine mesh with appropriate contact conditions and material properties. However, in the finite cavity pressure method, only the projectile was modeled with solid elements. The material property of the target and the contact between the target and the projectile was not considered. The interaction between the target and the projectile was the cavity pressure distribution with respect to only the cavity speed.

2.3. Free Surface Effect

The cavity pressure was calculated from the assumption that the target material is infinite. When the distance between the projectile and target is short, the pressure applied to the element is low compared to the normal. The free surface effect means that when the position of the projectile is near the ground, no pressure is generated because the cavity pressure is not perfectly formed at that part of the projectile. In order to consider the reduced cavity pressure on the surface near the target, Forrestal and Luk [13] proposed the following method.

In the calculation of the factor for the free surface effect, the aluminum material was considered as perfectly plastic and incompressible. In the calculation of the cavity pressure, a spherical cavity expansion problem with the infinite boundary and the finite boundary were employed. A schematic figure describing the free surface effect is presented in Figure 4. Warren and Poormon [17] derived the decay function, which is a function of d, a, and v and demonstrates the free surface effect.

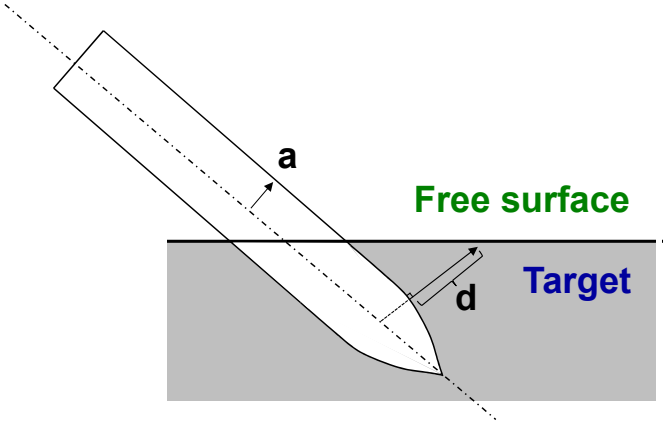

Figure 4. Schematic figure describing the free surface effect.

First, calculate the pressure acting at an infinite distance from the particle. Then calculate the pressure at a certain distance. The pressure ratio at a certain distance can be obtained through the air ratio. As shown in Figure 2, the interface between the elastic region and the plastic region should be defined. For an incompressible material, the elastic-plastic interface (b) is defined as follows:

$$\frac{a}{b} = \left(\frac{3Y}{2E}\right)^{1/3} \tag{3}$$

where *a* is the radius of the cavity. For metal materials, the pressure distribution depends on d. For the plastic region (d < b), the decaying function is defined as follows:

$$f(d,a,v) = \frac{2Y\ln\left(\frac{d}{a}\right) + \frac{1}{2}\rho v^2\left[3+\left(\frac{a}{d}\right)^4 - 4\left(\frac{a}{d}\right)\right]}{\frac{2Y}{3}\left[1+\ln\left(\frac{2E}{3Y}\right)\right] + \frac{3}{2}\rho v^2}, \quad d<b \tag{4}$$

For the elastic region (d ≥ b), the decaying function is defined as follows:

$$f(d,a,v) = \frac{\frac{2Y}{3}\left[\ln\left(\frac{2E}{3Y}\right)+1-\frac{2E}{3Y}\left(\frac{a}{d}\right)^3\right] + \frac{1}{2}\rho\dot{a}^2\left[3+\left(\frac{a}{d}\right)^4 - 4\left(\frac{a}{d}\right)\right]}{\frac{2Y}{3}\left[1+\ln\left(\frac{2E}{3Y}\right)\right] + \frac{3}{2}\rho v^2}, \quad d<b \tag{5}$$

Finally, the general solution according to d, a, and v is defined as follows:

$$\frac{\sigma_r(d,a,v)}{Y} = \left[A + B\left(\sqrt{\frac{\rho_0}{Y}}v\right) + C\left(\sqrt{\frac{\rho_0}{Y}}v\right)^2\right] f(d,a,v) \tag{6}$$

The aforementioned equation presents a cavity pressure distribution with respect to d_1 and v_1. The first equation presents the compressibility, strain hardening, and strain rate dependent cavity pressure of the aluminum materials. The following equation is the decaying function and presents the effects of the free surface effects.

3. Simulation Model

3.1. Geometries of the Projectile

In this study, various types of projectiles were employed in the penetration analysis. The projectile having an ogive nose geometry shown in Figure 5, was selected as the base geometry. The geometry of the projectile was divided into two parts: a body and a nose. The basic features are shown in Figure 5. The diameter of the projectile is 2a, and the value is 7.1 mm. The length of the

body is L_b, and the value is 59.3 mm. The ogive nose is defined with the caliber-radius-head (CRH) which is R/2a. When CRH is 3, the nose length (L_n) is 11.8 mm.

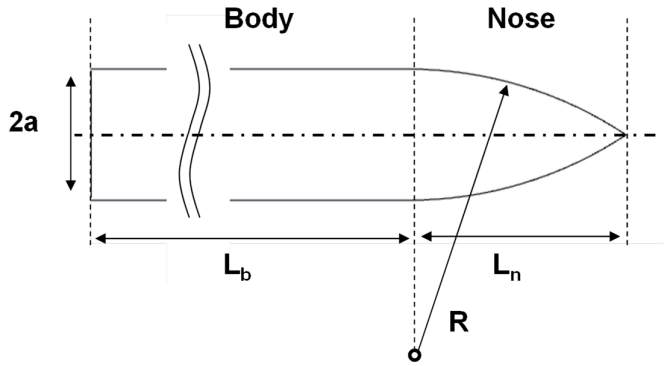

Figure 5. Geometry of the projectile having an ogive nose geometry.

Even if the geometries were changed, a and L_b were fixed. Only the length and geometry of the nose were modified. The projectiles with other geometries were compared to the aforementioned one. The conical geometry has the nose length (L_b) of a. The blunt geometry has the spherical geometry of the nose end, and the radius of the nose is a. For the blunt geometry, the CRH value is 0.5a. In addition, it was compared to a cylinder that has no nose geometry. The projectile having an ogive nose with CRH values of 1, 3, and 5 were also examined. The truncated geometry in Figure 6 has a half-height of the nose length of the projectile with an ogive nose with a CRH value of 3. In this paper, the projectiles with an ogive nose with CRH values of 1, 3, and 5 are noted as CRH=1, CRH = 3, and CRH = 5, respectively.

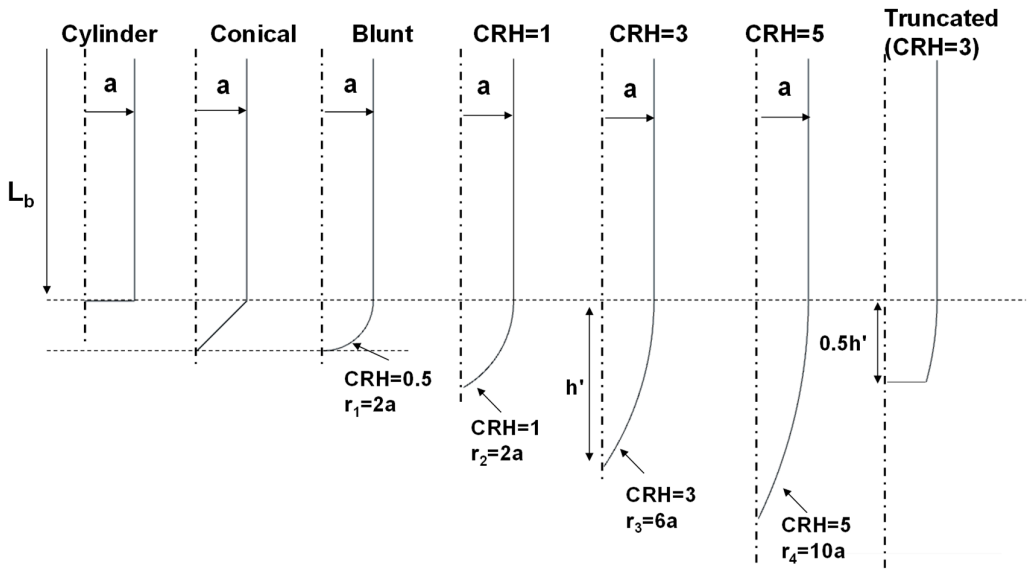

Figure 6. Compared geometries of the projectile.

The projectile material was vacuum-arc-remelted (VAR) 4340 steel [1]. The density of the material was 8000 kg/m^3. The stress-strain curve of the VAR 4340 steel is shown in Figure 7. The initial yield stress of the material in the quasi-static condition is 1430 MPa. When the projectile hits the target, the strain rate of the projectile is nearly 10^5 s^{-1}, which is very high value comparing with the quasi-static condition. As a result of the high strain rate, the strain rate dependent material properties shown in Figure 7 should be employed. In this work, the material property shown in Figure 7 was employed in ABAQUS/Explicit v6.13 using table type data. The reference strain rate

was 10^{-4} s^{-1}. The maximum strain rate in this work was 4×10^5 occurred in the normal impact of the cylinder geometry.

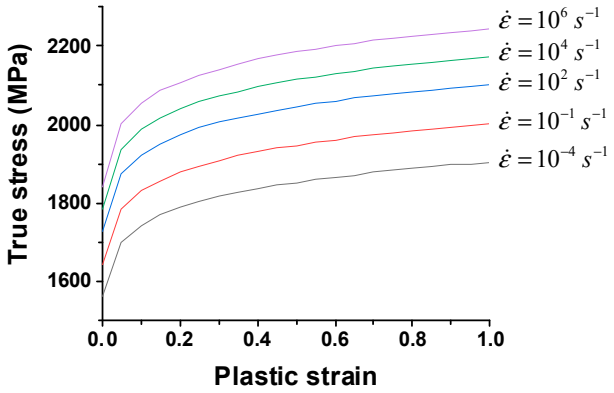

Figure 7. Material properties of vacuum-arc-remelted (VAR) 4340 with respect to strain rate [17].

3.2. Simulation Model

The simulation model for CRH = 3 is shown in Figure 8. In the simulation model with the finite cavity pressure method, only the projectile was modeled. In the finite element analysis, the cavity pressure is applied to the projectile when the projectile contacts with the target. Target is set to a point where the *y*-axis coordinates are less than zero. When the y-directional coordinate of the element is less than zero, the projectile is assumed to contact the target materials. In the analytical model below, the element is 1 mm in size, and 4176 C3D8R elements of ABAQUS/Explicit were used.

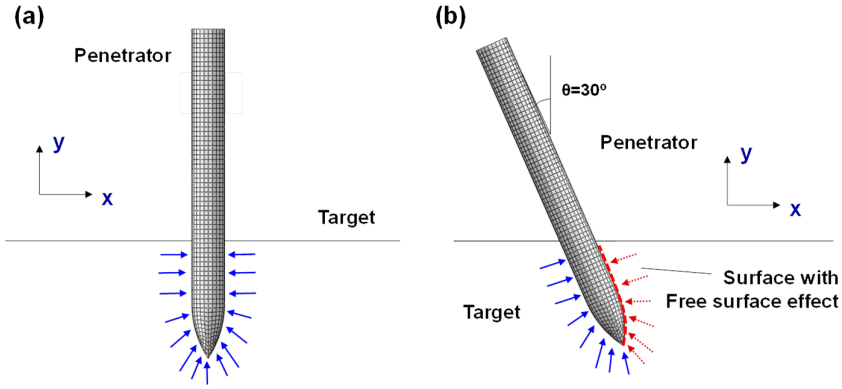

Figure 8. Simulation model for (**a**) normal penetration and (**b**) oblique penetration.

The oblique impact was modeled as shown in Figure 8b. With respect to the *x*-axis, the position of the projectile was rotated by the angle of impact. In Figure 8b, the rotating angle (θ) is 30°. Similarly, if the coordinate of the *y*-axis is less than 0, a collision is assumed to have occurred. Pressure has been considered to be applied by the cavity pressure from this point on. Moreover, the free surface effect occurs on the side close to the projectile and the ground; thus, a cavity pressure was applied using Equation (6). In the oblique impact, d in Figure 4, which is the distance between the free surface and the surface of the projectile, is very crucial, because d defines the value of the decay function in Equation (6). In the simulation, d was calculated using the surface normal of the corresponding element. After obtaining the normal direction of an element, the distance between an element and the free surface was calculated.

4. Results and Discussions

4.1. Verification Model

To verify the simulation model in this work, simulation results were compared to the penetration experiments of previous works. Warren and Poormon [17] examined an oblique impact test using the projectile having an ogive nose with the CRH value of 3 (CRH = 3) at various impact velocities and angles. The comparisons were conducted with the impact angle of 15° and 30°, which are presented in the previous works. Collision with the angle of 30° was analyzed for 1156 m/s and 753 m/s. Collision with the angle of 15° was investigated for 1209 m/s and 985 m/s. The target material was 6061-T6511 aluminum. The projectile material was VAR 4340 steel.

Under the conditions mentioned above, the results of the simulation and the experiment were listed in Table 1 and showed good agreements. The final coordinates of the projectile tip were (−39.1 mm, 130.7 mm) in the experimental result and (−37.1 mm, 129.55 mm) in the simulation result. Figure 9a presents the experimental result of the final deformed shape after impact for V = 985m/s, 15° angle of obliquity. Figure 9b presents the simulation result of the same conditions. The most significant difference was shown in the case of the impact angle of 30° and the velocity of 1156 m/s. In this case, the final position of the projectile tip showed an error of 17.25% in the Y-directional coordinate. In most other cases, the error is less than 5%. The analysis results showed that the analytical model of this study could predict the results of the experiment precisely considering the problems of measurement and experimental errors.

Table 1. Comparison of the positions of tip ends for various conditions.

Striking Velocity (m/s)	Angle of Obliquity (°)	Pitch (°)	Yaw (°)	Experimental Result [17]		Simulation Result	
				X (mm)	Y (mm)	X (mm)	Y (mm)
1156	30	3.25U	0	113.2	−149.5	106.83	−123.7
753	30	0.75D	0.25L	71.4	−55.2	69.89	−65.11
1209	15	0.75U	0.5L	70.5	−201.2	70.9	−191.5
985	15	2.5U	0.75L	39.1	−130.7	37.1	−129

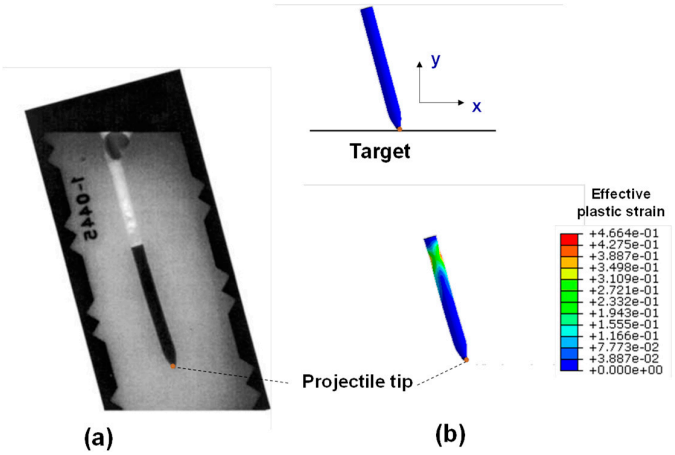

Figure 9. Final deformed shape after impact for V = 985 m/s, 15° angle of obliquity: (**a**) Experimental result [17] (**b**) Simulation result.

4.2. Simulation Results of the Normal Impact

In this study, the mass of the projectile varies, depending on the shape of the noses. The penetration characteristics of the projectile were analyzed with the penetration depth per mass of the projectile. The kinetic energy of the projectile was expressed as 0.5 mV^2. As the mass of the projectile increases, the kinetic energy proportionally increases. However, the kinetic energy by mass has the same value.

Also, as previously described, the penetration depth of an aluminum target (Al 6061-T6511) was analyzed. The velocity of the projectile was 1208 m/s for all cases. The penetration depth per mass is shown in Figure 10. The cylinder geometry showed the lowest value with the value of −1.21 m/kg. Blunt shape (−5.69 m/kg), conical shape (−6.23 m/kg), and truncated shape (−7.4 m/kg) are the next.

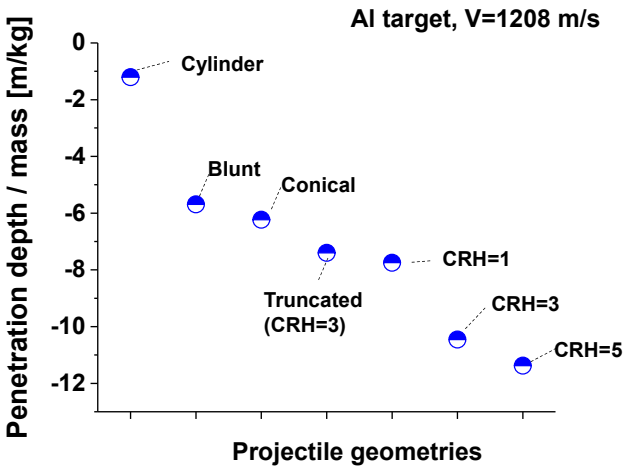

Figure 10. Penetration depth/mass distribution with respect to the projectile geometries.

Among seven projectile geometries, the projectile having the ogive nose showed increased penetration depth. Even with the same category of geometries, the penetration depth per mass varies significantly depending on the CRH value. The penetration depth to mass is 7.75 m/kg with a CRH of 1, 10.51 m/kg with a CRH of 3, and 11.47 m/kg with a CRH of 5.

4.3. Discussion-Effect of Plastic Deformation on the Normal Penetration

In the case of the normal impact, the projectile with an ogive nose showed the deepest penetration. The plastic deformation of the projectile has a significant effect on the penetration depth. The penetration depth of the projectile had a close relationship with its kinetic energy. Before the collision, the projectile had kinetic energy related to the velocity. If there was no energy loss, the kinetic energy changed to penetration energy and the deformation energy of the projectile. As the plastic deformation of the projectile increased, the deformation energy of the projectile increased. The remaining energy was converted into penetration energy.

Figure 11 shows the deformed shapes of the cylinder shape, blunt shape, truncated shape, and ogive shape with the CRH value of 3 (CRH = 3) in normal impact. The transmission depth is the highest in CRH = 3, followed by Truncated, Blunt, and Cylinder, as shown in Figure 10. In the case of the cylinder geometry, large plastic deformation occurs after impact. As a result, the shape of the projectile is significantly altered. The initial shape cannot be maintained. In the case of blunt geometry, the diameter of the projectile body was increased after impact. Plastic deformation at the tip of the projectile occurs in the truncated geometry, thereby increasing the lower diameter. However, in the case of CRH = 3, the plastic deformation at the center was also very small. The projectile retained its original shape.

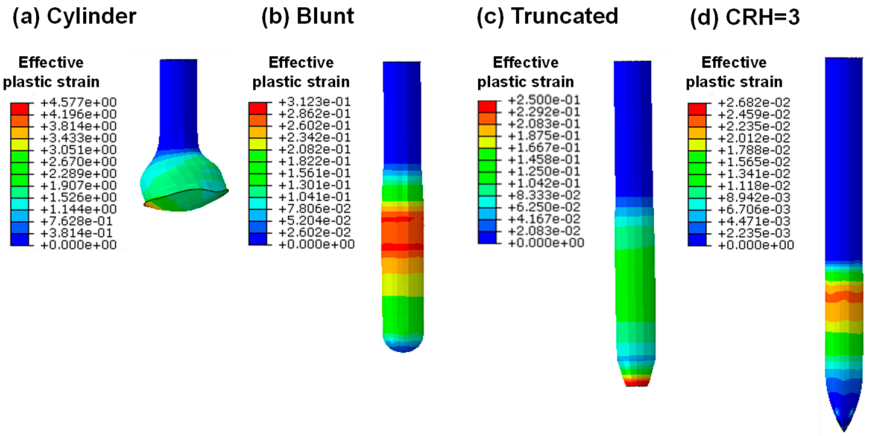

Figure 11. Deformation of the projectile after the normal penetration: (**a**) Cylinder, (**b**) Blunt, (**c**) Truncated, and (**d**) CRH = 3.

Figure 12 presents the velocity, and the displacement of the projectile tip for the cylinder geometry, blunt geometry, truncated geometry, and ogive geometry (CRH = 3). The velocity of the cylinder geometry reduced very quickly. Finally, the velocity of the projectile was converged to zero. For the projectile having an ogive nose (CRH = 3), showed a moderate reduction of the velocity. Consequently, the penetration depth was the largest. The reaction force of the projectile is proportional to the acceleration of the projectile. The cylinder geometry showed the largest acceleration, which is the first derivative of the velocity. It means that a large force occurred at the cylinder geometry.

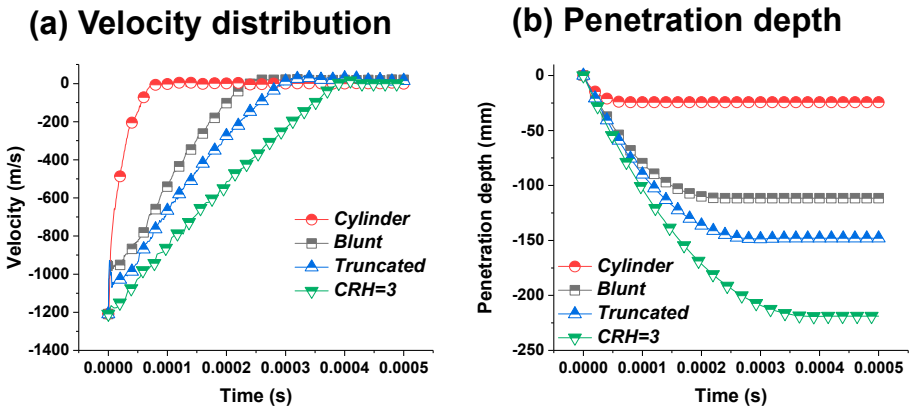

Figure 12. Velocity and penetration depth with respect to time: (**a**) Velocity distribution and (**b**) Penetration depth.

The graph in Figure 13 shows the relationship between the plastic deformation energy per mass and the depth of the penetration depth per mass. In Figure 11d, the maximum equivalent plastic strain is 0.027. The deformation energy of the projectile is very small. Therefore, the remained energy is converted to penetration energy and has good penetration performance. In the case of cylinder shape, plastic deformation is very large, indicating a large amount of plastic deformation energy. Before impact, all have kinetic energy relative to the same mass, where the larger the dispersion to plastic modified energy, the smaller the transmission depth can be found. If there were no nose in the projectile like the cylinder geometry, a strong reaction force due to the impact occurred at the earlier stage of the collision. This energy is converted into the plastic strain deformation of the material.

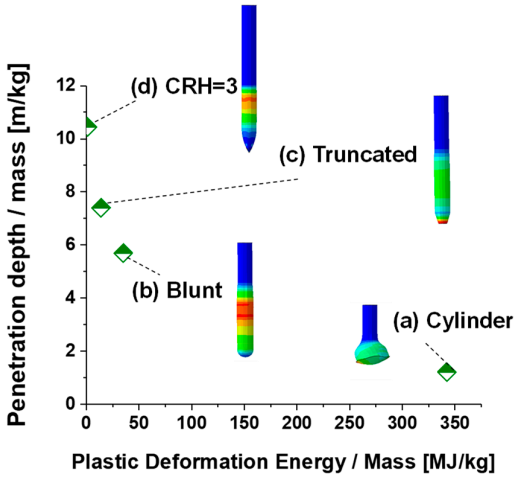

Figure 13. Relationship between penetration depth/mass and plastic deformation energy/mass: (**a**) Cylinder, (**b**) Blunt, (**c**) Truncated, and (**d**) CRH = 3.

In the case of the ogive shape, the angle of the nose between the surface of the nose and the center axis of the projectile is small. The cavity pressure occurred due to the impact is low compared to other cases. This greatly increases the depth of penetration. From these results, it was found that the geometry with large CRH value, which has a small angle between the surface of the nose and the center axis showed greater penetration. The deformation of the projectile is very small.

4.4. Simulation Results of the Oblique Impact

For the case of the oblique impact, the final position of the projectile tip was compared. If the position of the *x*-axis has a large value, it means that the projectile has moved a lot in the horizontal direction. Movement in the horizontal direction has an adverse effect on the penetration of the projectile. With the same kinetic energy, the ideal case is to penetrate in the travel direction. Figure 14 presents the coordinate of the projectile tip after impact with the velocity of 1208 m/s and the impact angle of 30°. The dash-dotted line in Figure 8 presents the line with an angle of 30°, which means the ideal result of the projectile movement. Additionally, the moving trajectories of the projectiles of various projectile geometries were presented in Figure 14.

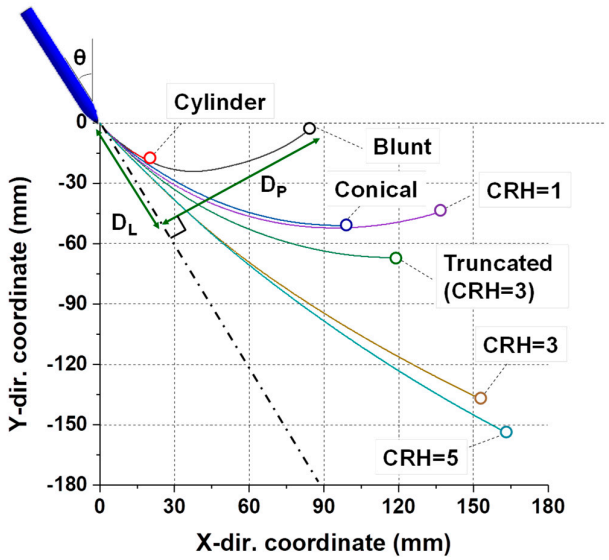

Figure 14. Trajectories of the projectiles and the final coordinates of the projectile tip with respect to the projectiles.

The simulation results of the oblique impact are summarized in Table 2. The final position of the projectile tip can be divided into two lengths. One is the length along the impact angle 30°, which is shown as D_L in Figure 14. Another is the perpendicular distance to the impact angle which is shown as D_P in Figure 14. The ratio of the displacement in the normal direction (D_P) to the displacement along the impact angle (D_L) is selected as a measurement which indicates whether the projectile followed the impact angle. When D_P/D_L is small, the projectile follows the impact angle. When D_P/D_L is large, the projectile moved to the perpendicular direction.

Table 2. Penetration depth concerning the projectile geometry in the oblique impact.

	Cylinder	Blunt	Conical	Truncated	CRH = 1	CRH = 3	CRH = 5
D_L/mass [m/kg]	1.472	2.025	4.657	5.632	5.035	9.007	9.748
D_P/mass [m/kg]	0.391	3.793	3.386	3.857	5.140	3.538	3.572
Ratio (D_P/D_L)	0.266	1.873	0.727	0.685	1.021	0.393	0.366

The cylinder geometry showed the smallest movement. The reaction forces due to the impact are very large. As a result, the plastic deformation of the projectile is also extensive. This is similar to the normal impact. For the blunt geometry, D_P/D_L showed the largest value among seven projectile geometries. It was shown that penetration depth is very low in the vertical direction and has moved in the horizontal direction. It means that the projectile cannot penetrate the target in the vertical direction. As the projectile moves, the projectile bends. Finally, the projectile moves along the bending direction.

Conical and truncated geometries do not move along the angle of impact. The bending deformation of the projectile occurred for the aforementioned cases. The ratios of the two cases (D_P/D_L) are close. However, the projectile with the truncated geometry showed better penetration characteristics.

The projectile with an ogive nose showed different results. For the projectile with an ogive nose with the CRH value of 1, the ratio is 1.021. The projectile moves similarly along the impact angle and the normal direction. Also, the bending deformation of the projectile occurred. However, if the CRH is 3 and 5, the projectile moves not far away from the impact angle. The ratio of the projectile (CRH = 3) is 0.393, and the projectile (CRH = 5) is 0.366. The blunt geometry is that the CRH value is 0.5. So, as the CRH value increases, the projectile moves more accurately along the impact angle. As the CRH value increases, the penetration depth of the projectile is increasing.

4.5. Effect of the Plastic Deformation on the Oblique Impact

The following figures show the deformed shape of various geometries after the oblique impact. In the case of the cylindrical shape, as soon as the projectile strikes, the pressure caused by the collision is concentrated at the end of the cylinder. The direction of the cavity pressure is normal to the bottom surface. Because of the pressure concentration at the bottom surface of the cylinder, the cylindrical projectile shows very large plastic deformation with compressive deformation as shown in Figure 15a.

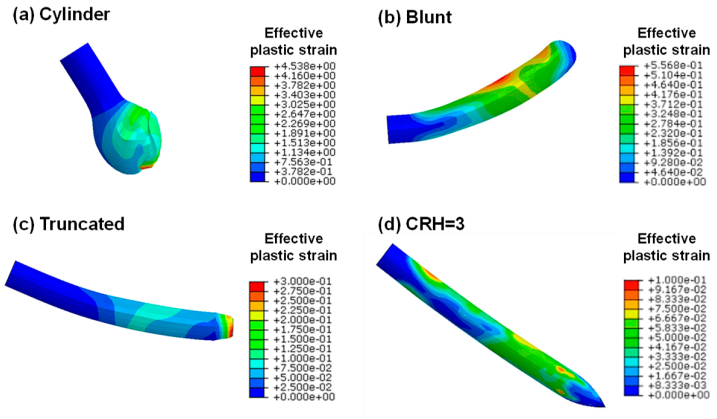

Figure 15. Deformation of the projectile after the oblique penetration; (**a**) Cylinder, (**b**) Blunt, (**c**) Truncated, and (**d**) CRH = 3.

For the blunt geometry, there was an asymmetric distribution of the cavity pressure because of the free surface effect, and the bending deformation of the projectile occurred. The maximum equivalent plastic strain was 0.557. The maximum plastic deformation occurred at the center of the projectile. Small pressure was applied to the projectile near the ground the projectile. However, on the opposite side, the depth of the target was considered as infinite, and full pressure was applied. Accordingly, the trajectory of the projectile shows 'J' curve. As the bending deformation increases, the projectile further moves horizontally. As bending deformation increases, the path of the projectile's movement follows the direction of the bending deformation. Accordingly, as shown in Figure 14, the final coordinate of the projectile in the horizontal direction greatly increased.

The projectile with a truncated geometry has a surface perpendicular to the moving direction. At that surface, the maximum plastic deformation occurred. The equivalent plastic strain was 0.295. Also, due to the asymmetric cavity pressure distribution, the bending deformation occurred. The deformed shape and final position of the projectile are shown in Figure 15c. Figure 15d presents the deformed shape and final position of the projectile having an ogive nose. The maximum plastic strain was 0.095, the smallest among four geometries. The bending deformation was very small, and thus, the penetration depth showed the largest value.

From the aforementioned results, the projectile geometry for improved penetration characteristics was studied. When the projectile has a surface perpendicular to the moving direction, the reaction forces from the impact are concentrated on that surface. Consequently, the deformation of the projectile occurred. The loss of the energy changed from kinetic energy to penetration energy. Under the normal impact and the oblique impact, the projectile having an ogive geometry shows the best penetration characteristics. As the CRH value increases, the penetration depth was also increased. Particularly for the oblique impact, as the CRH value increases, the bending deformation of the projectile decreases, thereby greatly increasing the penetration depth of the projectile.

5. Conclusions

In this work, the penetration characteristics of projectiles having a cylinder, conical, blunt, and ogive geometry were investigated using the finite cavity method. Normal and oblique impacts at an impact angle of 30° were compared. The target was a 6061-T6511 aluminum plate. And the material of the projectile was VAR 4340 steel. The projectile tended to be compressed in the normal impact and bent in the oblique impact. In both the normal impact and the oblique impact, the plastic deformation of the projectile had significant effects on the penetration. The cylinder having a surface perpendicular to the moving direction endured large stress during the earlier stage of the impact. Massive cavity pressure is applied on the surface having the normal direction to the velocity at the earlier stage of the impact. The reaction forces are very enormous; as a result, the acceleration of the projectile is large. Due to the concentrated force, large plastic deformation occurs. The projectile

having an ogive nose with a CRH value of 5 showed the smallest plastic deformation after impact and the best penetration performance. For the projectile having an ogive geometry, the length of the nose depended on the CRH value. As the CRH value increased, the length of the nose increased. At the same time, the angle of the tip between the center-axis of the projectile decreased. The decrease in the angle resulted in the cavity pressure at the projectile surface decreasing. Finally, the projectile having an ogive nose with high CRH value resulted in increased penetration depth.

Author Contributions: Y-H.Y.; methodology, project administration, writing, J-B.K.; review and editing, validation, C-W.L.; writing, methodology, conceptualization.

Funding: This work was supported by the Agency for Defense Development (No. UE161102GD) and the National Research Foundation of Korea (NRF) grant funded by the Korea government (MSIT) (No. NRF-2017R1C1B5017648).

Conflicts of Interest: The authors declare no conflict of interest.

Nomenclature

$\dot{\varepsilon}$	Strain rate (s^{-1})
ϱ_0	Density of the material (kg/m^3)
σ_r	Radial stress (MPa)
σ_θ	Hoop stress (MPa)
a	Radius of the projectile (m); Cavity radius (m)
b	Elastic-plastic interface (m)
CRH	Caliber Radius Head
d	Distance between the projectile surface and the free surface (m)
D_L	displacement along the impact angle (m)
D_P	displacement in the normal direction (m)
E	Elastic Modulus (GPa)
L_b	Length of the body (m)
L_n	Length of the nose (m)
$\vec{n}$	Normal vector of the element
R	Radius of the projectile nose (m)
v	Velocity of the particle (m/s)
Y	Yield strength of the material (MPa)

References

1. Wingrove, A.L. The influence of projectile geometry on adiabatic shear and target failure. *Metall. Trans.* **1973**, *4*, 1829–1833, doi:10.1007/bf02665409.
2. Huang, W.; Sheng, D.; Sloan, S.W.; Yu, H.S. Finite element analysis of cone penetration in cohesionless soil. *Comput. Geotech.* **2004**, *31*, 517–528, doi:10.1016/j.compgeo.2004.09.001.
3. Mahfuz, H.; Zhu, Y.; Haque, A.; Abutalib, A.; Vaidya, U.; Jeelani, S.; Gama, B.; Gillespie, J.; Fink, B. Investigation of high-velocity impact on integral armor using finite element method. *Int. J. Impact Eng.* **2000**, *24*, 203–217, doi:10.1016/S0734-743X(99)00047-0.

4. Rodriguez-Millan, M.; Garcia-Gonzalez, D.; Rusinek, A.; Abed, F.; Arias, A. Perforation mechanics of 2024 aluminium protective plates subjected to impact by different nose shapes of projectiles. *Thin Walled Struct.* **2018**, *123*, 1–10, doi:10.1016/j.tws.2017.11.004.
5. Young, C. *Penetration equations (SAND 97-2426)*. Sandia Natl. Lab. Albuquerque, NM, USA, 1997.
6. Young, C. *Simplified Analytical Model of Penetration with Lateral Loading—Users Guide*; Applied Research Associates, Inc.: Albuquerque, NM, USA, 1998.
7. Forrestal, M.J.; Luk, V.K. Penetration into soil targets. *Int. J. Impact Eng.* **1992**, *12*, 427–444, doi:10.1016/0734-743X(92)90167-R.
8. Forrestal, M.J.; Tzou, D.Y. A spherical cavity-expansion penetration model for concrete targets. *Int. J. Solids Struct.* **1997**, *34*, 4127–4146, doi:https://doi.org/10.1016/S0020-7683(97)00017-6.
9. Forrestal, M.J.; Tzou, D.Y.; Askari, E.; Longcope, D.B. Penetration into ductile metal targets with rigid spherical-nose rods. *Int. J. Impact Eng.* **1995**, *16*, 699–710, doi:10.1016/0734-743X(95)00005-U.
10. Warren, T.L.; Forrestal, M.J. Effects of strain hardening and strain-rate sensitivity on the penetration of aluminum targets with spherical-nosed rods. *Int. J. Solids Struct.* **1998**, *35*, 3737–3753, doi:10.1016/S0020-7683(97)00211-4.
11. Chen, X.W.; Li, Q.M. Deep penetration of a non-deformable projectile with different geometrical characteristics. *Int. J. Impact Eng.* **2002**, *27*, 619–637, doi:10.1016/S0734-743X(02)00005-2.
12. He, T.; Wen, H.M.; Qin, Y. Finite element analysis to predict penetration and perforation of thick FRP laminates struck by projectiles. *Int. J. Impact Eng.* **2008**, *35*, 27–36, doi:10.1016/j.ijimpeng.2006.11.008.
13. Macek, R.W.; Duffey, T.A. Finite cavity expansion method for near-surface effects and layering during Earth penetration. *Int. J. Impact Eng.* **2000**, *24*, 239–258, doi:10.1016/S0734-743X(99)00156-6.
14. Fang, Q.; Kong, X.; Hong, J.; Wu, H. Prediction of projectile penetration and perforation by finite cavity expansion method with the free-surface effect. *Acta Mech. Solida Sin.* **2014**, *27*, 597–611, doi:10.1016/S0894-9166(15)60005-2.
15. Kong, X.; Fang, Q.; Wu, H.; Zhang, Y. Finite Spherical Cavity Expansion Method for Layering Effect. *Acta Mech. Solida Sin.* **2016**, *29*, 642–654, doi:10.1016/S0894-9166(16)30334-2.
16. Bishop, R.F.; Hill, R.; Mott, N.F. The theory of indentation and hardness tests. *Proc. Phys. Soc.* **1945**, *57*, 147–159, doi:10.1088/0959-5309/57/3/301.
17. Warren, T.L.; Poormon, K.L. Penetration of 6061-T6511 aluminum targets by ogive-nosed VAR 4340 steel projectiles at oblique angles: Experiments and simulations. *Int. J. Impact Eng.* **2001**, *25*, 993–1022, doi:10.1016/S0734-743X(01)00024-0.